The solution structure of the N-terminal domain of E3L shows a tyrosine conformation that may explain its reduced affinity to Z-DNA *in vitro*

Jan D. Kahmann*, Diana A. Wecking*, Vera Putter*, Ky Lowenhaupt†, Yang-Gyun Kim†‡, Peter Schmieder§, Hartmut Oschkinat§, Alexander Rich†¶, and Markus Schade*¶

*Combinature Biopharm AG and §Forschungsinstitut für Molekulare Pharmakologie, Robert-Rössle-Strasse 10, D-13125 Berlin, Germany; †Department of Biology, Massachusetts Institute of Technology, 77 Massachusetts Avenue, Cambridge, MA 02139; and ‡Department of Biochemistry, College of Medicine, Chung-Ang University, 221 Heuksuk-Dong, Dongjak-ku, Seoul 156-756, Korea

Contributed by Alexander Rich, December 23, 2003

The N-terminal domain of the vaccinia virus protein E3L ($Z\alpha_{E3L}$) is essential for full viral pathogenicity in mice. It has sequence similarity to the high-affinity human Z-DNA-binding domains $Z\alpha_{ADAR1}$ and $Z\alpha_{DLM1}$. Here, we report the solution structure of $Z\alpha_{E3L}$ and the chemical shift map of its interaction surface with Z-DNA. The global structure and the Z-DNA interaction surface of $Z\alpha_{E3L}$ are very similar to the high-affinity Z-DNA-binding domains $Z\alpha_{ADAR1}$ and $Z\alpha_{DLM1}$. However, the key Z-DNA contacting residue Y48 of $Z\alpha_{E3L}$ adopts a different side chain conformation in unbound $Z\alpha_{E3L}$, which requires rearrangement for binding to Z-DNA. This difference suggests a molecular basis for the significantly lower *in vitro* affinity of $Z\alpha_{E3L}$ to Z-DNA compared with its homologues.

Vaccinia virus is a member of the large double-stranded DNA family of poxviruses. It has been used globally as a vaccine to eradicate smallpox, a devastating disease caused by variola virus that is presently an important threat of bioterrorism (1). The vaccinia virus protein E3L, which is conserved in variola and related viruses, plays a key role in circumventing the IFN-mediated defense of host cells (2). E3L contains two domains, of which the C-terminal double-stranded RNA-binding domain is essential and sufficient for evading IFN host defense in cultured cells. In animal models, however, full pathogenesis requires the N-terminal domain of E3L (2), which has sequence homology to the family of Z-DNA-binding protein domains ($Z\alpha$) but shows only comparatively low affinity to Z-DNA *in vitro* (3). When the $Z\alpha_{E3L}$ domain is removed from vaccinia virus and is replaced by either $Z\alpha_{ADAR1}$ or $Z\alpha_{DLM1}$, the virus retains full pathogenicity in the mouse model. Mutational studies show that these domains bind to Z-DNA (4).

The structurally defined $Z\alpha$ domains are 62-residue (α plus β) helix–turn–helix proteins with an additional β-sheet that bind to left-handed Z-DNA with medium nanomolar affinity *in vitro* (5, 6). The 3D structures of the human $Z\alpha$ domains of the RNA-editing enzyme ADAR1 ($Z\alpha_{ADAR1}$) and of the tumor-related protein DLM1 ($Z\alpha_{DLM1}$) were solved complexed with Z-DNA (7, 8). Further, the solution structure of $Z\alpha_{ADAR1}$ was determined in the unbound state (9), and residues essential for binding to Z-DNA were identified by alanine-scanning mutagenesis (5). Single-point mutations in two such residues, which strongly reduce the affinity of $Z\alpha_{ADAR1}$ to Z-DNA *in vitro*, were recently shown to abrogate vaccinia virus pathogenicity in a mouse model when introduced in homologous positions in the N-terminal domain of E3L ($Z\alpha_{E3L}$) (4). Considering this close correlation in the function of such residues between $Z\alpha_{ADAR1}$ and $Z\alpha_{E3L}$ the lack of correlation in their *in vitro* affinity to Z-DNA is intriguing.

Here, we report the solution structure of $Z\alpha_{E3L}$ and a chemical shift map of its interaction surface with Z-DNA. The 3D structure and interaction surface of $Z\alpha_{E3L}$ is grossly very similar to $Z\alpha_{ADAR1}$ and $Z\alpha_{DLM1}$ but differs in the side chain conformation of a pivotal Z-DNA-contacting residue Y48. In contrast to $Z\alpha_{ADAR1}$ and $Z\alpha_{DLM1}$, Y48 of free $Z\alpha_{E3L}$ is exposed to solvent and shows selective vanishing of its NMR signals consistent with a conformational rearrangement when Z-DNA is bound. Therefore, the additional cost in energy for rearranging Y48 may account for the substantially lower *in vitro* affinity of $Z\alpha_{E3L}$ to Z-DNA as compared with its homologues $Z\alpha_{ADAR1}$ and $Z\alpha_{DLM1}$. *In vivo*, this energy may be provided by other factors, rendering wild-type $Z\alpha_{E3L}$–E3L as pathogenic as the $Z\alpha_{ADAR1}$–E3L chimera (4).

Materials and Methods

Protein Preparation. Residues 1–78 of the vaccinia virus gene E3L (GenBank no. AAA02759), comprising the $Z\alpha_{E3L}$ domain, with four additional vector-encoded residues at the N terminus, were expressed as a fusion protein with an N-terminal $(His)_6$ tag from a pET-28 vector (Novagen) in *Escherichia coli* strain BL21(DE3). Alternatively, residues 5–70 of E3L were expressed similarly for DNA interaction assays.

To produce ^{15}N- and $^{15}N/^{13}C$-labeled $Z\alpha_{E3L}$, bacteria were grown in M9 medium containing 1 g/liter $^{15}NH_4Cl$ and 1.5 g/liter ^{13}C-glucose. Cultures were induced with 1 mM isopropyl β-D-thiogalactoside (IPTG) when they reached OD_{600} of 0.8. After 4 h induction, cells were harvested, resuspended in 50 mM NaH_2PO_4 (pH 8.0), 300 mM NaCl, 10 mM imidazole, supplemented with Roche Complete Protease Inhibitor Mix, and lysed by French pressing. The lysate was centrifuged at 48,000 $\times$ *g* for 30 min. The supernatant was applied on a Ni-NTA column (Qiagen, Hilden, Germany). After washing with 50 mM NaH_2PO_4 (pH 8.0), 300 mM NaCl, 20 mM imidazole, the $(His)_6$ tag protein attached to the Ni^{2+} matrix was eluted by thrombin digestion overnight at room temperature in PBS. The cleaved protein was loaded on a Resource Q column (Amersham Biosciences), and the bound protein was eluted with a gradient of 0–1 M NaCl (20 mM NaH_2PO_4, pH 6.5). Alternatively, bacteria were lysed with Bugbuster (Novagen) following the manufacturer's protocol, and protein was purified as described (4). Briefly, the $(His)_6$-fusion protein was purified by using HisBind resin (Novagen). Bound protein was stepped off with 300 mM imidazole in 500 mM NaCl, 20 mM Tris (pH 8.0). The $(His)_6$ tag was removed by thrombin digestion for 3 h at room temperature in 20 mM Tris·HCl (pH 8.0), 150 mM NaCl, 2.5 mM $CaCl_2$, 1 mM EDTA. $Z\alpha_{E3L}$ protein was further purified by using a HiTrap Q column (Amersham Biosciences) and a 25–500 mM NaCl gradient. Matrix-assisted laser desorption ionization–time

Abbreviations: $Z\alpha$, Z-DNA-binding protein domain; HSQC, heteronuclear single quantum coherence; NOE, nuclear Overhauser enhancement.

Data deposition: The atomic coordinates of the 20 lowest energy structures of a total of 450 have been deposited in the Protein Data Bank, www.pdb.org (PDB ID code 1OYI).

¶To whom correspondence may be addressed. Fax: 617-253-8699 (A.R.). E-mail: schade@combinature.com (M.S.).

© 2004 by The National Academy of Sciences of the USA

of flight (MALDI-TOF) mass spectrometry of the ^{15}N- and $^{15}N/^{13}C$-labeled $Z\alpha_{E3L}$ yielded single peaks at 9,291 Da and 9,672 Da, respectively, which agree very well with the calculated molecular masses of 9,292 Da and 9,685 Da, respectively.

NMR Spectroscopy. NMR experiments were carried out at 25°C on 2.2-mM u-^{15}N-labeled and 2-mM u-^{13}C,^{15}N-labeled $Z\alpha_{E3L}$ samples in 20 mM sodium-phosphate (pH 6.5), 20 mM NaCl, 0.1 mM NaN_3 with 5% and 100% D_2O, respectively, on 600-MHz NMR spectrometers. ^1H, ^{15}N, and ^{13}C resonance assignments were obtained from the following 3D heteronuclear correlation experiments (10): CBCA(CO)NH, CBCANH, HBHA(CO)NH, H(CCO)NH, C(CCO)NH, HCCH-COSY, and HCCH-TOCSY. Interproton distance restraints were derived from 3D ^{15}N-heteronuclear single quantum coherence (HSQC)-NOESY (150-ms mixing time), 3D ^{13}C-HSQC-NOESY (40 and 70 ms mixing times). Spectra were processed with XWINNMR (Bruker) and analyzed with SPARKY 3.105 (11). Spectra were referenced by external calibration on 2,2-dimethyl-silapentane-5-sulfonic acid (DSS), sodium salt (12).

Interaction Mapping. For interaction mapping, a shortened $Z\alpha_{E3L}$ construct (comprising residues 5–70 of GenBank no. AAA02759) was used that lacks the first four N-terminal and the last eight C-terminal residues. These residues are nonstructured in the 3D structure of $Z\alpha_{E3L}$. The ^1H and ^{15}N backbone chemical shifts are virtually identical between this construct and the 1–78 residues construct, indicating that both constructs share the same 3D fold. 1D ^1H and 2D ^{15}N-HSQC NMR spectra were recorded on the following four samples in 20 mM [bis(2-hydroxyethyl)amino]tris(hydroxymethyl)methane (Bistris; pH 6.7), 50 mM NaCl, 5% D_2O at 25°C: (*i*) 40 μM $Z\alpha_{E3L}$, (*ii*) 40 μM $Z\alpha_{E3L}$ with 300 μM $[Co(NH_3)_6]^{3+}$, (*iii*) 40 μM $Z\alpha_{E3L}$ with 10 μM $d(CG)_6T_4(CG)_6$, and (*iv*) 40 μM $Z\alpha_{E3L}$ with 10 μM $d(CG)_6T_4(CG)_6$ and 300 μM $[Co(NH_3)_6]^{3+}$. After NMR data acquisition, CD spectra were recorded on each sample at room temperature by using a 2-mm cuvette on a Jasco J-720 CD spectrometer (Jasco, Easton, MD). CD control spectra of 10 μM $d(CG)_6T_4(CG)_6$ in the B-DNA conformation and in the Z-DNA conformation were recorded in a 1-mm cuvette at room temperature in 20 mM Bistris (pH 6.7), 50 mM NaCl buffer alone, and with 5 M NaCl, respectively. The assignments and concentration dependence of the chemical shift changes of $Z\alpha_{E3L}$ were confirmed by a titration experiment on a 20-μM $Z\alpha_{E3L}$ sample with increasing concentrations of $d(CG)_6T_4(CG)_6$ (1, 2, 4, 7, and 12 μM) and a constant $[Co(NH_3)_6]^{3+}$ over DNA excess of 30 in 20 mM Bistris (pH 6.7), 50 mM NaCl, and 5% D_2O at 25°C. Spectra were processed and analyzed as described above. Chemical shift changes were averaged according to the formula $[(\Delta^1H)^2 + (\Delta^{15}N/5)^2]^{0.5}$ (13).

Structure Calculation. Nuclear Overhauser enhancement (NOE) distance restraints derived from ^{15}N- and ^{13}C-edited NOESY experiments were manually assigned and further analyzed (calibration and removal of redundant distance restraints) by using the program DYANA 3.1 (14). Seventy-two backbone dihedral angle constraints were derived from Cα chemical shifts according to the rules (15): $-120° < \psi < -20°$ and $-100° < \phi < 0°$ for $\Delta(C\alpha) > 1.5$ ppm, and $-200° < \psi < -80°$ and $40° < \phi < 220°$ for $\Delta(C\alpha) < -1.5$ ppm. The dihedral angle constraints are in agreement with the preliminary structure calculated solely from the NOE restraints. Further 20 hydrogen bonds within α-helices and four hydrogen bonds within β-strands were derived from the NOE-based preliminary structure and confirmed by the analysis of the Cα and Cβ chemical shift values by using the program TALOS (16). Structures were calculated by 4,000 steps of simulated annealing with torsion angle dynamics and subsequently 1,000 steps of minimization in DYANA 3.1. For better convergence during structural refinement, the ψ and ϕ dihedral angles of the residues 59, 60, and 61 preceding the cis peptide bond between I62 and P63 were preset to a range that is wider by 5° or more than the range of the structural ensemble calculated without such preset angles.

Table 1. Structural statistics

NOE upper distance limits*	487
Dihedral angle constraints*	78
Residual target function, Å²*†	0.9 ± 0.1
Residual distance constraint violations*†‡	
Number ≥ 0.1 Å	5.5 ± 0.3
Maximum, Å	0.24 ± 0.05
Residual dihedral angle constraint violations*†	
Number ≥ 2 deg	0 ± 0
Maximum, deg	0.1 ± 0.1
rms deviations from ideal geometry§	
Bond lengths, Å	0.01
Bond angles, deg	1.7
rms deviation from the mean coordinates†¶	
Backbone (N, Ca, C), Å	0.8 ± 0.2
All heavy atoms, Å	1.6 ± 0.2
Ramachandran analysis†¶	
Residues in most favored regions	72.5%
Residues in additional allowed regions	22.6%
Residues in generously allowed regions	4.8%
Residues in disallowed regions	0.1%

*Calculated ensemble (residues 5–70) (GenBank accession no. AAA02759).
†Mean value ± SD of the ensemble of 20 independently calculated conformers.
‡No distance constraint violation ≥ 0.2 Å in six or more structures.
§Submitted ensemble (residues 9–70) (PDB ID code 1OYI).
¶Core domain (residues 11–68).

Results and Discussion

Structure Determination. The 3D structure of the N-terminal Z-DNA-binding domain of the vaccinia virus gene product E3L (residues 1–78) was determined by multidimensional NMR spectroscopy in solution. Complete chemical shift assignments were obtained from 3D triple-resonance and double-resonance NMR spectra except for the first two vector-encoded residues. Chemical shifts of residues 1–10 and 69–78 are not well dispersed. This finding is confirmed by the 3D structure demonstrating that the folded core domain comprises residues 11–68 (subsequently referred to as $Z\alpha_{E3L}$). Residues 9–10 and 69–70 show a preferred orientation, as evidenced by a few medium-range NOE, whereas all other N- and C-terminal residues are unstructured. Structural statistics are listed in Table 1. The coordinates of the ensemble of the 20 lowest energy structures of $Z\alpha_{E3L}$ (residues 9–70) have been deposited in the Protein Data Bank with the PDB ID code 1OYI.

Structure Description. The $Z\alpha_{E3L}$ domain is composed of three α-helices (designated $\alpha1$, $\alpha2$, and $\alpha3$) and three β-strands (designated $\beta1$, $\beta2$, and $\beta3$) in an $\alpha1\beta1\alpha2\alpha3\beta2\beta3$ linear order (Fig. 1). Helices $\alpha1$ and $\alpha3$ pack against a short anti-parallel, triple-stranded β-sheet, in which $\beta3$ is sandwiched between $\beta1$ and $\beta2$. Strands $\beta1$ and $\beta3$ are connected by only two backbone hydrogen bonds between residues A27 and W66. Strands $\beta2$ and $\beta3$ are bridged by three hydrogen bonds comprising residues Y57 and S59 of $\beta2$ and R65 and F67 of $\beta3$. The ensemble of the 20 lowest energy structures shows that only loop 2 between $\alpha2$ and $\alpha3$ is less rigid whereas all other loops are tightly structured rendering $Z\alpha_{E3L}$ a rigid body. Loop 4 between $\beta2$ and $\beta3$ is made rigid by the two sequential prolines 63 and 64, of which the former adopts a rare cis peptide bond. The side chains of the

BIOCHEMISTRY

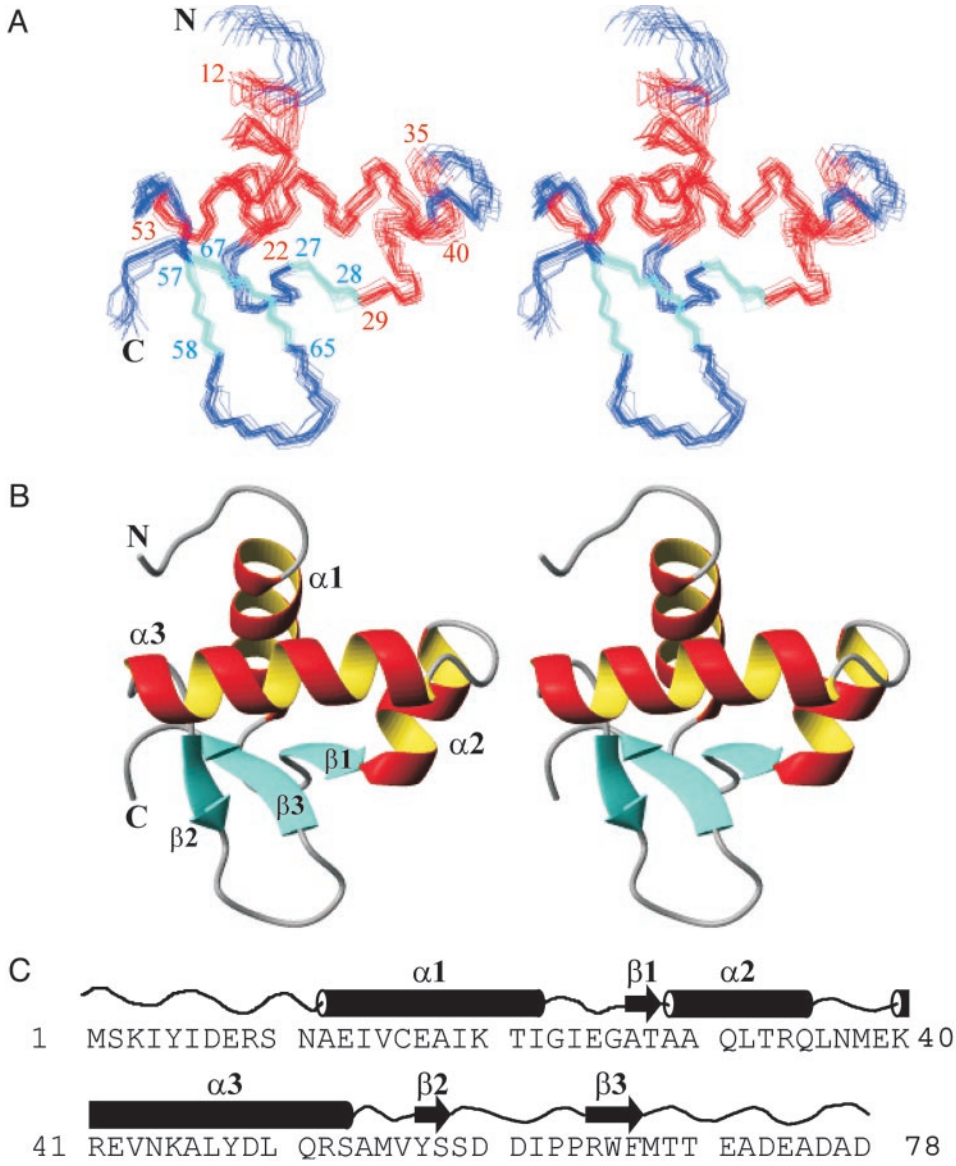

Fig. 1. 3D solution structure of $Z\alpha_{E3L}$. (*A*) Stereoview of the ensemble of the 20 lowest energy structures of E3L. The first and last residue of the 3 α-helices (red) (α1, α2, α3) and 3 β-strands (cyan) (β1, β2, β3) are numbered. (*B*) Stereoview of the backbone ribbon of the mean structure illustrating the (α plus β) helix–turn–helix fold of $Z\alpha_{E3L}$. The N- and C-termini are labeled with N and C, respectively. (*C*) The secondary structure of $Z\alpha_{E3L}$ is shown with the amino acid sequence directly under it.

other residues in this loop (D60, D61, I62, and R65) are flexible in the structural ensemble, giving this loop the shape of a solvent accessible finger with a rigid backbone. Mutational (5) and structural studies (7, 9) have demonstrated that this distinctly conserved feature is essential for selective interaction of the homologous $Z\alpha_{ADAR1}$ domain with Z-DNA. In the co-crystal structure of $Z\alpha_{ADAR1}$ and Z-DNA, the protein makes several important van der Waals contacts to Z-DNA.

Chemical Shift Mapping of the E3L/Z-DNA Interaction Surface. Alternating $d(CG)_n$ oligomers have been successfully used to study the interaction of the Z-DNA-binding domains $Z\alpha_{ADAR1}$ (7, 9) and $Z\alpha_{DLM1}$ (8) with Z-DNA. In contrast to these high-affinity Z-DNA-binding homologues, $Z\alpha_{E3L}$ does not flip the B-DNA conformation of these substrates into the Z-conformation when incubated with each other under physiological buffer conditions at micromolar concentrations (3). The CD spectrum of 40 μM $Z\alpha_{E3L}$ in the presence of 10 μM $d(CG)_6T_4(CG)_6$ clearly indicates a B-DNA conformation for this DNA substrate (Fig. 2*A*, blue curve). Further, the 2D ^{15}N-HSQC NMR spectrum of this sample shows no chemical shift changes when compared with the spectrum of the protein alone (see Fig. 4, which is published as supporting information on the PNAS web site). This result indicates that $Z\alpha_{E3L}$ does not interact with $d(CG)_6T_4(CG)_6$ in the B-DNA conformation under these conditions because chemical shifts are sensitive even to weak interactions.

To investigate the interaction between $Z\alpha_{E3L}$ and $d(CG)_6T_4(CG)_6$ in the Z-DNA conformation, $[Co(NH_3)_6]^{3+}$, which is known to promote the conversion from B- to Z-DNA (17), was added to a final concentration of 300 μM under otherwise identical conditions. The CD spectrum of this sample shows large alterations of the molar ellipticity at 295 and 255 nm, which are characteristic for $d(CG)_n$ oligomers in a left-handed Z-DNA conformation (Fig. 2*A*, red curve). The corresponding ^{15}N-HSQC NMR spectrum shows a large number of chemical

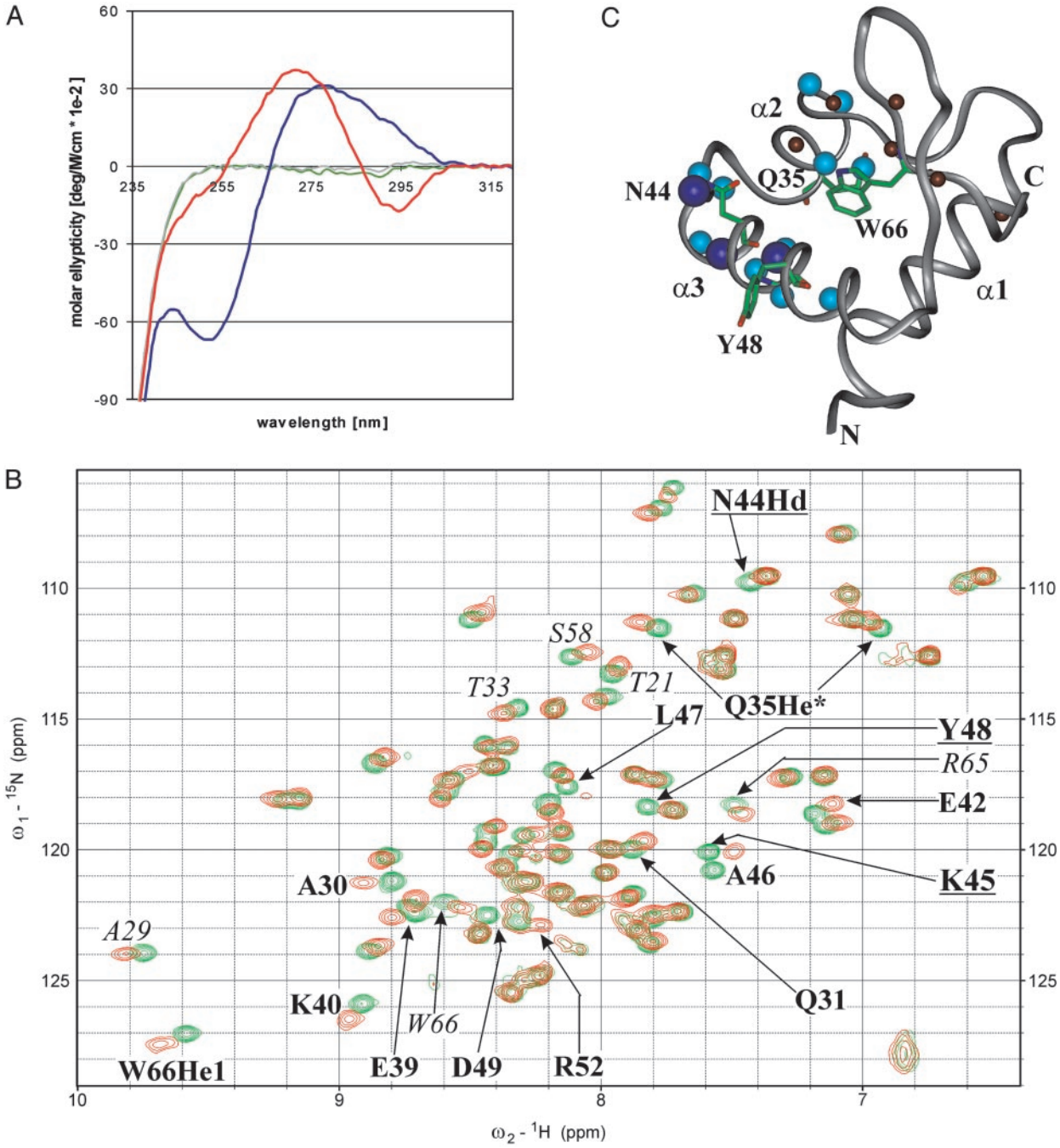

Fig. 2. (*A*) The conformation of substrate DNA in the presence of $Z\alpha_{E3L}$. The CD spectrum of $d(CG)_6T_4(CG)_6$ substrate DNA in the presence of $Z\alpha_{E3L}$ (blue curve) shows a conventional B-DNA conformation. In contrast, the CD spectrum of $d(CG)_6T_4(CG)_6$ in the presence of $Z\alpha_{E3L}$ and $[Co(NH_3)_6]^{3+}$, which is known to promote the conversion from B- to Z-DNA (17), shows an inversion of ellipticity at 295 and 255 nm characteristic for duplex DNA in the Z-conformation (red curve). For control, $Z\alpha_{E3L}$ alone (green curve) and $Z\alpha_{E3L}$ in the presence of $[Co(NH_3)_6]^{3+}$ (gray curve) show zero ellipticity between 320 and 250 nm. (*B*) Chemical shift map of the $Z\alpha_{E3L}$/substrate DNA interaction. The ^{15}N-HSQC NMR spectrum of $Z\alpha_{E3L}$ in the presence of $d(CG)_6T_4(CG)_6$ and $[Co(NH_3)_6]^{3+}$ (red peaks) shows several large chemical shift changes compared with $Z\alpha_{E3L}$ alone (green peaks). In addition, there are three vanishing resonances (residues underlined). This finding indicates a selective interaction between $Z\alpha_{E3L}$ and $d(CG)_6T_4(CG)_6$ in the vicinity of the affected residues. The ^{15}N-HSQC NMR spectrum of $Z\alpha_{E3L}$ in the presence of $d(CG)_6T_4(CG)_6$ substrate DNA shows no chemical shift alterations as compared with $Z\alpha_{E3L}$ alone (Fig. 4), indicating no discernible interaction under these conditions. Further, the spectrum of $Z\alpha_{E3L}$ in the presence of $[Co(NH_3)_6]^{3+}$ is identical to $Z\alpha_{E3L}$ alone (not shown). (*C*) The Z-DNA-binding site of $Z\alpha_{E3L}$. In the presence of $d(CG)_6T_4(CG)_6$ and $[Co(NH_3)_6]^{3+}$, the H atoms of $Z\alpha_{E3L}$ that show large averaged chemical shift changes ($\geq$0.082 ppm; bold labels in *B*) are shown as cyan spheres. H atoms with medium shifts ($\geq$0.068 ppm; italic labels in *B*) are shown as dark red spheres. Atoms of $Z\alpha_{E3L}$ that show vanishing resonances (underlined labels in *B*) are shown as dark blue spheres in the 3D structure of $Z\alpha_{E3L}$. Chemical shifts are listed in Table 2, which is published as supporting information on the PNAS web site. These data indicate a contiguous Z-DNA-binding site made up of helices α3 and α2 and the area around W66.

shift changes and three vanishing signals (Fig. 2*B*) with respect to $Z\alpha_{E3L}$ alone, indicating that $Z\alpha_{E3L}$ interacts with $d(CG)_6T_4(CG)_6$ in the Z-DNA conformation. The concentration dependence of these chemical shift alterations has been confirmed by an independent chemical shift-mapping experiment at 20 μM $Z\alpha_{E3L}$ with increasing $d(CG)_6T_4(CG)_6$ concen-

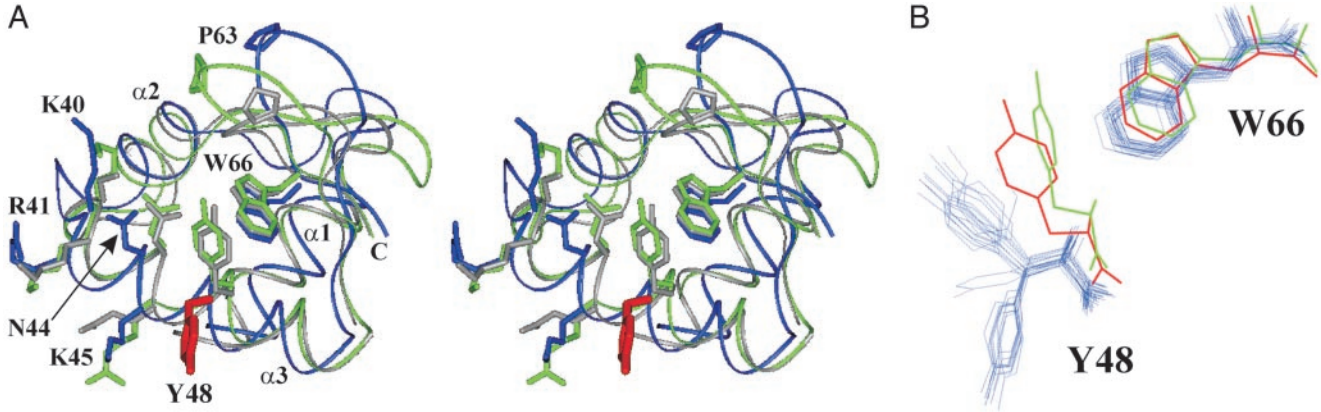

Fig. 3. Superposition of the 3D structures of $Z\alpha_{E3L}$ (blue), $Z\alpha_{ADAR1}$ (light green), and $Z\alpha_{DLM1}$ (gray) in stereo. (*A*) The secondary structure elements of $Z\alpha_{E3L}$, $Z\alpha_{ADAR1}$, and $Z\alpha_{DLM1}$ superimpose well except for the loop containing P63 (side chain labeled). Also, the side chains of K40, R41, N44, K45, and W66, which contact the bound Z-DNA in the co-crystal structures of $Z\alpha_{ADAR1}$ and $Z\alpha_{DLM1}$, show very similar positions. Only the side chain of Y48 adopts a distinct position in $Z\alpha_{E3L}$ (red) as compared with $Z\alpha_{ADAR1}$ and $Z\alpha_{DLM1}$. (*B*) Distinct Y48-W66 distance between $Z\alpha_{E3L}$ and $Z\alpha_{ADAR1}$. Superposition of Y48 and W66 between the 20 lowest energy structures of E3L (blue), unbound $Z\alpha_{ADAR1}$ (red), and bound $Z\alpha_{ADAR1}$ (light green). Whereas Y48 residues are within van-der-Waals distance to W66 in both $Z\alpha_{ADAR1}$ structures, it adopts two solvent exposed rotamer positions in $Z\alpha_{E3L}$, which are 7.2 and 10.8 Å apart from W66.

trations at a constant $[Co(NH_3)_6]^{3+}$ to $d(CG)_6T_4(CG)_6$ ratio of 30 (Fig. 5, which is published as supporting information on the PNAS web site).

The ^1H and ^{15}N chemical shift perturbations were quantified and averaged (see Table 2). The atoms showing averaged perturbations $\geq$0.068 ppm are displayed in the 3D structure of unbound $Z\alpha_{E3L}$ (Fig. 2*C*). The chemical shift changes map to a contiguous surface encompassing helix α3, the N terminus of helix α2, and the indole proton Hε of W66. The three vanishing signals, which are indicative of intermediate exchange between bound and unbound $Z\alpha_{E3L}$ on the NMR time scale, comprise the backbone amides of Y48 and K45 and the Hδ21 proton of N44 (Figs. 2*B* and 5). The other side-chain amide proton of N44, Hδ22, does not vanish, suggesting a selective interaction with the Hδ21 proton. The only other shift changes in side-chain amides were observed for the two Hε21 and Hε22 protons of Q35, which are located within a suitable distance for a water-mediated hydrogen bond to the carbonyl of Q31. The backbone amide of Q31 at the N terminus of helix α2 also shows a strong chemical shift alteration. Therefore, the shift changes in the side chain of Q35 probably reflect subtle rearrangements at the N terminus of α2 when Z-DNA is bound rather than direct contact with the Z-DNA. Contacts with the sequential prolines 63 and 64 are not discernible by this mapping method because prolines lack protons bound to nitrogen. Taken together, chemical shift mapping by ^{15}N-HSQC NMR indicates that $Z\alpha_{E3L}$ selectively interacts with DNA in the left-handed Z-conformation through residues in helices α3 and α2 and strand β3, with prominent side-chain perturbations in atoms Hδ21 of N44 and Hε of W66. This result suggests that $Z\alpha_{E3L}$ utilizes a Z-DNA interaction surface that is globally very similar to those of its homologues $Z\alpha_{ADAR1}$ and $Z\alpha_{DLM1}$ (7, 8).

The Backbone Structure of $Z\alpha_{E3L}$ Is Similar to $Z\alpha_{ADAR1}$ and $Z\alpha_{DLM1}$. As expected from the primary sequence homology between $Z\alpha_{E3L}$, $Z\alpha_{ADAR1}$, and $Z\alpha_{DLM1}$, the three Z-DNA-binding domains share the same $\alpha1\beta1\alpha2\alpha3\beta2\beta3$ topology. The structure of $Z\alpha_{E3L}$ shows a backbone rms deviation of 1.24 Å to $Z\alpha_{ADAR1}$ and of 1.21 Å to $Z\alpha_{DLM1}$ (superposition of helices and strands only), indicating that the sequence homology is paralleled by a high overall structural homology. In particular, the three α-helices and three β-strands overlay very well between $Z\alpha_{E3L}$, $Z\alpha_{ADAR1}$, and $Z\alpha_{DLM1}$ (Fig. 3*A*). Structural differences are observed for the loops connecting α1 and β1 (loop 1), α2 and α3 (loop 2), and β2 and β3 (loop 4), of which the latter shows the most marked deviation in its backbone conformation. This finding is not unexpected because loop 4 contains profound differences on the primary sequence level. In $Z\alpha_{DLM1}$ loop 4 (all subsequent amino acid numbers refer to the homologous residues of $Z\alpha_{E3L}$) is shorter by two residues than in $Z\alpha_{E3L}$ and $Z\alpha_{ADAR1}$. Moreover, the six residues preceding P63 of loop 4 are poorly conserved between $Z\alpha_{E3L}$ and $Z\alpha_{ADAR1}$. The cis proline 63 of this loop is the sole conserved residue in $Z\alpha_{E3L}$, $Z\alpha_{ADAR1}$, and $Z\alpha_{DLM1}$. Proline 63 is of particular importance for the Z-DNA-binding activity because it confers direct Z-DNA contacts in the co-crystal structures of $Z\alpha_{ADAR1}$ (7) and $Z\alpha_{DLM1}$ (8). Furthermore, the strongest loss of virulence is found when this residue is mutated to alanine in wild-type $Z\alpha_{E3L}$ (4). In the 3D structures of $Z\alpha_{E3L}$ and $Z\alpha_{ADAR1}$, P63 adopts identical positions at the tip of loop 4 although in $Z\alpha_{E3L}$ the entire loop 4 is rotated away from helix α3, resulting in a distance of $\approx$5.9 Å between the N atoms of P63 of $Z\alpha_{E3L}$ and $Z\alpha_{ADAR1}$. This offset in the interaction surface may be compensated by a subtle adjustment in the binding geometry between $Z\alpha_{E3L}$ and Z-DNA. In conclusion, the overall backbone structure of $Z\alpha_{E3L}$ is very similar to its homologues $Z\alpha_{ADAR1}$ and $Z\alpha_{DLM1}$, with the exception of loop 4, which shows a displacement that is not expected to markedly affect binding to Z-DNA.

Y48 Adopts a Distinct Conformation in $Z\alpha_{E3L}$. To provide a molecular understanding for the significantly lower affinity of $Z\alpha_{E3L}$ to Z-DNA as compared with $Z\alpha_{ADAR1}$ and $Z\alpha_{DLM1}$, the structural comparison of the Z-DNA contacting residues between these homologues is of paramount interest. Of the total of eight common Z-DNA-contacting residues in the co-crystal structures of $Z\alpha_{ADAR1}$ and $Z\alpha_{DLM1}$, the three residues P63, P64, and W66 possess rigid side chains whose conformations are identical between $Z\alpha_{ADAR1}$ and $Z\alpha_{E3L}$ within the limitations of the backbone comparison described above. Of the remaining five Z-DNA contacting residues in helix α3, the side chains of K40, R41, N44, and K45 adopt similar positions in $Z\alpha_{E3L}$, $Z\alpha_{ADAR1}$, and $Z\alpha_{DLM1}$ (Fig. 3*A*). Only the side chain of Y48 is markedly different, showing a distinct solvent exposed conformation in $Z\alpha_{E3L}$. A closer view of Y48 and W66 in the ensemble of the 20 lowest energy structures of $Z\alpha_{E3L}$ superimposed on $Z\alpha_{ADAR1}$ and $Z\alpha_{DLM1}$ demonstrates (Fig. 3*B*) that the phenolic ring of Y48 probably adopts two major rotamer positions, which are $\approx$7.2 Å and 10.8 Å apart from W66 (distance Y48(Cz) − W66(Cz2)). In

contrast, the Y48 − W66 distance in bound (9) and unbound $Z\alpha_{ADAR1}$ (7) measures only 3.9 and 4.5 Å, respectively. The experimental foundation of this marked difference is the observation of several long-range NOEs between the aromatic rings of Y48 and W66 in the NMR structure of unbound $Z\alpha_{ADAR1}$ but none of such NOEs in the ^{13}C-edited NOESY spectra of $Z\alpha_{E3L}$. Neither does Y48 of $Z\alpha_{E3L}$ show long-range NOEs to other residues. The general sensitivity of the NOESY experiments on $Z\alpha_{E3L}$ is confirmed by the observation of 21 long-range NOEs for the aromatic protons of W66. Therefore, Y48 of $Z\alpha_{E3L}$ adopts two flexible solvent-exposed rotamer positions whereas Y48 of $Z\alpha_{ADAR1}$ is tightly packed against W66 in both the unbound and bound state.

In the co-crystal structures of $Z\alpha_{ADAR1}$ and $Z\alpha_{DLM1}$, Y48 is the only residue that mediates direct contacts to a base of the bound Z-DNA. In this interaction, the base adopts the *syn* conformation, which is characteristic for the left-handed Z-conformation of double-stranded DNA. This close interaction geometry suggests that in $Z\alpha_{E3L}$ the solvent-exposed side chain of Y48 rearranges when $Z\alpha_{E3L}$ binds to Z-DNA. By analyzing resolved ^1H chemical shifts in $1D^1H$-NMR spectra of 20 μM $Z\alpha_{E3L}$ with increasing concentrations of $d(CG)_6T_4(CG)/[Co(NH_3)_6]^{3+}$, we found that the aromatic Hδ and Hε atoms of Y48 vanish when $Z\alpha_{E3L}$ binds to Z-DNA. Moreover, the chemical shifts of both methyl groups of L47 (−0.21 and −0.314 ppm in unbound $Z\alpha_{E3L}$), which are packed in van-der-Waals distance underneath the indole ring of W66, alter in this experiment. These data indicate that the chemical environment around the side chains of L47, Y48, and W66 changes when Z-DNA is bound. Further, the observation of selectively vanishing signals for the HN, Hδ, and Hε of Y48 and the HN of K45 (Fig. 5), which is connected to HN of Y48 through an (i, i + 3) α-helical hydrogen bridge, is in agreement with conformational rearrangements of the Y48 when $Z\alpha_{E3L}$ binds to Z-DNA. The cost in energy for such a rearrangement may account for the substantially lower affinity of $Z\alpha_{E3L}$ to Z-DNA, as compared with $Z\alpha_{ADAR1}$ and $Z\alpha_{DLM1}$, where Y48 is prepositioned to bind Z-DNA (9).

Mutational experiments suggest that Y48 plays a key role for both binding to Z-DNA *in vitro* as well as viral pathogenicity in mice. In $Z\alpha_{ADAR1}$, the mutation of Y48 to alanine leads to both a profound loss in Z-DNA affinity and a significant reduction in binding specificity to the Z-conformation of DNA, as evidenced by Biacore and CD spectroscopy (4, 5, 7). In $Z\alpha_{E3L}$, the mutation of Y48 to alanine abrogates viral pathogenicity in mice by three $\log_{10}$ units (4). It is therefore intriguing to consider Y48 a conformational switch that has to be turned inward toward the protein to enable binding to Z-DNA. *In vivo*, this switch may be turned on by activating proteins and induced by preformed segments of Z-DNA.

The importance of the tyrosine–Z-DNA interaction is further illustrated by a second domain in ADAR-1 called $Z\beta_{ADAR1}$. Although it has many sequence similarities to $Z\alpha_{ADAR1}$, it lacks the tyrosine on helix 3, has an isoleucine instead, and shows no *in vitro* Z-DNA binding (3, 4). When put into vaccinia virus instead of $Z\alpha_{E3L}$, the chimeric virus shows no pathogenicity (4). However, if a mutant $Z\beta_{ADAR}$ is made, changing isoleucine to tyrosine, it then binds Z-DNA *in vitro*, and the chimeric virus becomes pathogenic.

A yeast one-hybrid system has been developed in which reporter gene (β-galactosidase) expression depends on binding of a protein to Z-DNA near the promoter (3). The protein is fused to a transcriptional activator domain, which turns on the gene. When $Z\alpha_{E3L}$ is used, the response of the reporter gene is the same as when $Z\alpha_{ADAR1}$ or $Z\alpha_{DLM1}$ are used (3). As with vaccinia virus infection, this yeast *in vivo* system shows that $Z\alpha_{E3L}$ is active in binding Z-DNA. The experiments reported here suggest that residue Y48 undergoes a conformational change on binding Z-DNA *in vitro*. Thus, the change in the tyrosine side chain conformation may act as a switch to turn on *in vivo* activity.

We thank Heidemarie Lerch and Eberhard Krause for matrix-assisted laser desorption ionization–time of flight (MALDI-TOF) mass spectrometry and Heike Nikolenko and Michael Bienert for providing a CD spectrometer. We further thank T. D. Goddard, G. Cornilescu and F. Delaglio, and P. Güntert for providing the software SPARKY 3.105, TALOS, and DYANA 3.1/MOLMOL 2.1–2.6, respectively. This work was supported by grants from the National Institutes of Health (to A.R.).

1. Cohen, J. (2001) *Science* **294,** 985.
2. Brandt, T. A. & Jacobs, B. L. (2001) *J. Virol.* **75,** 850–856.
3. Kim, Y. G., Lowenhaupt, K., Oh, D. B., Kim, K. K. & Rich, A. (2004) *Proc. Natl. Acad. Sci. USA*, in press.
4. Kim, Y. G., Muralinath, M., Brandt, T., Pearcy, M., Hauns, K., Lowenhaupt, K., Jacobs, B. L. & Rich, A. (2003) *Proc. Natl. Acad. Sci. USA* **100,** 6974–6979.
5. Schade, M., Turner, C. J., Lowenhaupt, K., Rich, A. & Herbert, A. (1999) *EMBO J.* **18,** 470–479.
6. Schade, M., Behlke, J., Lowenhaupt, K., Herbert, A., Rich, A. & Oschkinat, H. (1999) *FEBS Lett.* **458,** 27–31.
7. Schwartz, T., Rould, M. A., Lowenhaupt, K., Herbert, A. & Rich, A. (1999) *Science* **284,** 1841–1845.
8. Schwartz, T., Behlke, J., Lowenhaupt, K., Heinemann, U. & Rich, A. (2001) *Nat. Struct. Biol.* **8,** 761–765.
9. Schade, M., Turner, C. J., Kuhne, R., Schmieder, P., Lowenhaupt, K., Herbert, A., Rich, A. & Oschkinat, H. (1999) *Proc. Natl. Acad. Sci. USA* **96,** 12465–12470.
10. Cavanagh, J., Fairbrother, W. J., Palmer, A. G. & Skelton, N. J. (1996) *Protein NMR Spectroscopy* (Academic, San Diego).
11. Goddard, T. D. & Kneller, D. G. (2002) SPARKY 3 (University of California, San Francisco).
12. Markley, J. L., Bax, A., Arata, Y., Hilbers, C. W., Kaptein, R., Sykes, B. D., Wright, P. E. & Wuthrich, K. (1998) *J. Mol. Biol.* **280,** 933–952.
13. Shuker, S. B., Hajduk, P. J., Meadows, R. P. & Fesik, S. W. (1996) *Science* **274,** 1531–1534.
14. Guntert, P., Mumenthaler, C. & Wuthrich, K. (1997) *J. Mol. Biol.* **273,** 283–298.
15. Spera, S., Ikura, M. & Bax, A. (1991) *J. Biomol. NMR* **1,** 155–165.
16. Cornilescu, G., Delaglio, F. & Bax, A. (1999) *J. Biomol. NMR* **13,** 289–302.
17. Behe, M. & Felsenfeld, G. (1981) *Proc. Natl. Acad. Sci. USA* **78,** 1619–1623.